# Valence-shell double photoionization of alkaline-earth-metal atoms

A. S. Kheifets*
*Research School of Physical Sciences, The Australian National University, Canberra, Australian Capital Territory 0200, Australia*

Igor Bray†
*ARC Centre for Matter-Antimatter Studies, Murdoch University, Perth 6150 Australia*

(Received 12 December 2006; revised manuscript received 18 February 2007; published 11 April 2007)

We apply the convergent close-coupling formalism to describe direct double photoionization (DPI) of the valence $ns^2$ shell of alkaline-earth-metal atoms: beryllium ($n=2$), magnesium ($n=3$), and calcium ($n=4$). We consider the range of photon energies below the onset of resonant and Auger ionization processes where the subvalent and core electrons can be treated as spectators. By comparing alkaline-earth-metal atoms with helium, we elucidate the role of the ground state and final ionized state correlations in DPI of various quasi-two-electron atoms.

DOI: 10.1103/PhysRevA.75.042703 PACS number(s): 32.80.Fb, 31.25.Eb

## I. INTRODUCTION

Theoretical and experimental studies of direct double photoionization (DPI) of atomic targets beyond helium gained considerable momentum in recent years. The direct DPI process, in contrast to its resonant or Auger counterparts, is driven entirely by many-electron correlations and therefore is ideally suited to study electron correlations in atoms. Alkaline-earth-metal atoms are attractive targets for these studies because of their relatively simple quasi-two-electron structure. In these atoms, the outer valence shell is well separated from the rest of the atom. Therefore, at relatively small photon energies, the inner core and subvalent electrons can be treated as "spectators," not taking direct part in photoionization of the outer valence shell. In this situation, the DPI process in alkaline-earth-metal atoms is similar to that in He except for a different radial structure of the target *ns* orbital and the influence of the distorting potential on the departing photoelectrons.

Beryllium is an archetypal quasi-two-electron system in which the separation of the valence and core orbitals is very well pronounced both in the coordinate space, $\langle r\rangle_{1s}=0.41$ a.u., $\langle r\rangle_{2s}=2.65$ a.u., and in energy $\epsilon_{1s}=-4.73$ a.u., $\epsilon_{2s}=-0.31$ a.u. Here the Hartree-Fock values of the mean electron radii and the one-electron energies are calculated using the computer code of Dyall *et al.* [1]. In addition to the simple electronic structure, beryllium has an extended energy range from its double-ionization threshold at 27.53 eV [2] up to around 115 eV in which resonant or Auger mechanisms do not contribute to the DPI process.

The first experimental observation of the direct valence shell DPI of Be was reported by Wehlitz and Whitfield [3] who measured the double-to-single photoionization cross-section ratio between the photon energies of 32 and 80 eV. At about the same time, but independently, the theoretical ratio was reported by Kheifets and Bray [4] who employed a frozen core model and treated Be as a He-like target within the convergent close-coupling (CCC) formalism. A good agreement between theory and experiment was found in subsequent analysis of the data [5]. The CCC results were also later confirmed by hyperspherical *R*-matrix with semiclassical outgoing waves (HRM-SOW) [6] and time-dependent close-coupling (TDCC) [7] calculations. Very recently, Wehlitz and collaborators [5,8] studied DPI of Be below the photon energy of 40 eV with much improved statistics and energy resolution. The new set of data for the DPI cross section was found in agreement with the CCC and TDCC calculations. Close examination of the experimental DPI cross section near threshold revealed quite an unexpected oscillating structure which was at variance with the Wannier law and attributed to the Coulomb dipole field of the singly ionized target [9].

More interest in the direct DPI of beryllium was generated by a recent theoretical study of the angular correlation in the two-electron continuum in the ground state and metastable He and other two-electron targets [10]. It was argued that because DPI near threshold would proceed mainly via electron-impact ionization of the singly ionized target, the width of the angular correlation function in DPI was determined by the Compton profile of the target electron bound to the singly charged ion. This mechanism could explain the considerable narrowing of the angular correlation function in Be as compared to He. An alternative explanation of this effect was proposed by Citrini *et al.* [6] who attributed it to a stronger ground-state correlation in beryllium as compared to helium.

Direct valence shell DPI in heavier alkaline-earth-metal atoms (Mg, Ca, Sr) is studied to a much lesser extent. Osawa *et al.* [11] announced their measurement of the double-to-single cross-section ratio $\sigma^{2+}/\sigma^{+}$ for Ca and Sr in the photon energy range from the double-ionization threshold (17.99 eV for Ca and 16.73 eV for Sr) to just below the lowest excited state of the subvalent shell (30 eV for Ca and 24.5 eV for Sr). These data, however, are still to be published. Direct DPI of Ca was studied by Beyer *et al.* [12] who measured the fully resolved triply differential cross section (TDCS) at equal energy sharing between the photoelectrons and ob-

*URL: http://rsphysse.anu.edu.au/~ask107. Electronic address: A.Kheifets@anu.edu.au
†URL: http://atom.murdoch.edu.au. Electronic address: I.Bray@murdoch.edu.au

 

served a marked difference from similar data in He.

Theoretically, direct DPI from Mg and Ca was first studied by Ceraulo *et al.* [13] within a theoretical scheme which took into account the final-state electron correlation by introducing a Coulomb hole factor. However, this approach for He failed to provide even qualitative agreement with the experimental data. Kazansky and Ostrovsky [14] calculated direct DPI in Be, Mg, Ca, and Sr by employing an extended Wannier ridge model and mimicking the ground-state correlation by introducing a Coulomb hole in the initial state. This theory predicted a double-hump angular correlation function (reduced TDCS in the author's terminology) for all studied atoms. This prediction was not confirmed in subsequent CCC calculations for Be [4].

Valence shell DPI was studied experimentally in the region of the giant $3p \rightarrow 3d$ resonance in Ca [15,16] and $4p \rightarrow 4d$ resonance in Sr [17,18]. The Ca measurements were analyzed in subsequent theoretical papers [14,19,20]. These studies, however, go beyond the scope of the present work.

In this paper, we concentrate on direct valence shell DPI of Be, Mg, and Ca in the range of photon energies from the threshold to the lowest excitation from the core (Be) or nearest subvalent shell (Mg and Ca). The motivation of this work is to study systematically a range of quasi-two-electron atoms and to elucidate the role of the ground- and final-state correlations in DPI process. In particular, we want to shed more light on the issue of angular correlation width in the two-electron continuum. We present more evidence that the narrowing of the angular correlation width from light to heavy alkaline-earth-metal atoms is related to the shrinking *ns* orbital in the momentum space which corresponds to a more diffuse orbital in the coordinate space shielded from the nucleus by inner electrons.

In the present work, we use essentially the same theoretical scheme as was employed in our earlier calculation on Be [4]. Although some results for Be were reported previously, we feel it necessary to include beryllium in the present study for systematics and because a large amount of good quality experimental data became available thus enabling us to subject the theory to a more stringent test.

The body of the present paper is organized as follows. In Sec. II we give a brief outline of our theoretical model. In Sec. III A we present our results for the integrated single and double photoionization cross sections. In Secs. III B and III C, we analyze the DPI amplitudes and fully differential photoionization cross sections. In Sec. IV we conclude by summarizing our findings and presenting a unifying picture of DPI of alkaline-earth-metal atoms and helium.

## II. FORMALISM

### A. Multiconfiguration Hartree-Fock ground state

We assume the *LS* coupling scheme and make the following configuration-interaction expansion of the $ns^2\ ^1S$ valence shell:

$$\Psi_0(\boldsymbol{r}_1,\boldsymbol{r}_2) = \sum_{l=0}^{l_{\max}} \sum_{m=n}^{n_{\max}} C_{ml} |\phi_{ml}(\boldsymbol{r}_1)\phi_{ml}(\boldsymbol{r}_2):{}^1S\rangle. \tag{1}$$

The multiconfiguration Hartree-Fock (MCHF) orbitals $\phi_{ml}(\boldsymbol{r})$ are found in the static-exchange potential of the frozen core with the electron configuration of He, Ne, and Ar for Be ($n=2$), Mg ($n=3$), and Ca ($n=4$), respectively. Only diagonal $ml^2$ terms are included in expansion (1) as is always the case for the MCHF ground state. This is so because a HF ground state is stable with respect to the one-electron–one-hole excitations and the first nonvanishing correction should be of the two-electron–two-hole type.

TABLE I. Ground-state properties of helium and alkaline-earth-metal atoms.

| $n$ | 1 | 2 | 3 | 4 |
|---|---|---|---|---|
| Atom | He | Be | Mg | Ca |
| Expansion | MCHF15 | MCHF13 | MCHF17 | MCHF15 |
| $l_{\max}$ | 4 | 3 | 4 | 4 |
| $n_{\max}$ | 5 | 5 | 6 | 6 |
| $R_m^\infty$ (%) $m=1$ | 94.541 | | | |
| 2 | 4.469 | 94.578 | | |
| 3 | 0.564 | 4.817 | 94.738 | |
| 4 | 0.188 | 0.374 | 4.741 | 94.928 |
| 5 | 0.086 | 0.114 | 0.330 | 4.645 |
| 6 | 0.047 | 0.051 | 0.098 | 0.279 |
| 7 | 0.029 | 0.028 | 0.043 | 0.080 |
| 8 | 0.019 | 0.017 | 0.023 | 0.035 |
| $R_\infty$ | 1.758 | 0.370 | 0.256 | 0.175 |
| $C_{ns^2}$ | 0.996 | 0.954 | 0.965 | 0.959 |
| $\Delta V_{\text{ion}}^{\text{HF}}/V_{\text{ion}}$ (%) | 1.4 | 4.5 | 5.9 | 8.6 |
| $\Delta V_{\text{ion}}^{\text{MCHF}}/V_{\text{ion}}$ (%) | 0.01 | 0.48 | 1.9 | 4.1 |

The coefficients in the MCHF expansion (1) are found by using the MCHF computer code [1]. The number of terms in the MCHF expansion is increasing until we are satisfied with the stability of the ground-state energy and, more importantly, the asymptotic photoionization ratios taken in the limit of infinite photon energy:

$$R_m^\infty = \left.\frac{\sigma_m}{\sigma^+ + \sigma^{++}}\right|_{\omega\to\infty} = \frac{c_m}{c}, \quad R_\infty = \left.\frac{\sigma^{++}}{\sigma^+}\right|_{\omega\to\infty} = \frac{c - \sum_m c_m}{\sum_m c_m}, \tag{2}$$

where $\sigma_m$ is a single-photoionization cross section corresponding to an $m$ final ion state, and $\sigma^+ = \Sigma_{m=n}^\infty \sigma_m$ and $\sigma^{2+}$ are the total single- and double-photoionization cross sections. In Eq. (2), we introduce the following overlap integrals [21]:

$$c_m \propto |\langle \phi_{ms}^+ | \delta(\boldsymbol{r}_2) | \Psi_0 \rangle|^2, \quad c \propto |\langle \Psi_0 | \delta(\boldsymbol{r}_2) | \Psi_0 \rangle|^2, \tag{3}$$

where $\phi_{ms}^+$ is the one-electron *ms* orbital of the singly charged ion.

Results for $R_m^\infty$ and $R_\infty$ are shown in Table I. For comparison, we also show the corresponding parameters for the ground-state He. Although the limit of infinite photon energy has no physical meaning for valence shell photoionization, we may use the asymptotic ratios as indicators of the relative strength of various single- and double-photoionization channels at finite photon energies. In particular, Pattard [22] pro-

posed a universal shape function which bridges from the low-energy Wannier behavior to the high-energy Bethe-Born theory:

$$\frac{\sigma^{2+}}{\sigma^{+}}(E) = R_\infty \frac{E^\alpha (E+E_0)^{7/2}}{(E+E_1)^{7/2}}, \tag{4}$$

where $\alpha = 1.056$ is the Wannier exponent and $E_0$ and $E_1$ are the fitting parameters. The shape function (4) was used successfully by Wehlitz *et al.* [5] to describe the experimental double-to-single photoionization cross-section ratio in Be.

We see that the asymptotic ratio $R_\infty$ is decreasing systematically from He to Ca. This is related to the fact that the overlaps between the corresponding orbitals bound to the neutral atom and the singly charged ion $\langle ns \| ns^+ \rangle$ are increasing from He to Ca which, in turn, is related to the shielding action of the core. This increases the relative probability of the target electron to remain bound and, therefore, decreases the probability of the double photoionization. A monotonic decrease in asymptotic ratios $R_\infty$ from He to Mg is actually translated into decreasing double-to-single ratios at finite photon energies as will be shown in the following sections. The only exception from this sequence is Ca which has the smallest asymptotic ratio but the largest double-to-single ratio at finite photon energies.

Other entries in Table I serve to indicate the comparative strength of the ground-state correlation in He and alkaline-earth-metal atoms. The coefficient $C_{ns^2}$ is accompanying the leading $ns^2$ configuration in the MCHF expansion (1). Deviation of this coefficient from unity indicates the admixture of other configurations to the noncorrelated Hartree-Fock ground state. The ground-state correlation can also be quantified in terms of the correlation energy or, more specifically, the relative shift of the theoretical Hartree-Fock double-ionization potential with respect to the experimental one, $\Delta V_{\rm ion}^{\rm HF}/V_{\rm ion}$. By both counts, He is the least correlated atom which is bound tightly by the Coulomb force of the bare nucleus. As the nucleus becomes shielded, the strength of the ground-state correlation is gradually increasing from Be to Ca.

The last entry in Table I is the relative shift of the theoretical MCHF double-ionization potential with respect to the experimental one, $\Delta V_{\rm ion}^{\rm MCHF}/V_{\rm ion}$. It gives an indication of the accuracy of the MCHF expansion achieved with a given number of terms.

### B. CCC formalism

The photoionization cross section, as a function of the photon energy $\omega$, corresponding to a particular bound electron state $j$ of the ionized target is given by [23]

$$\sigma_j(\omega) = \frac{4\pi^2}{\omega c} \sum_{m_j} \int d^3k_b \left| \langle \Psi_j^{(-)}(\boldsymbol{k}_b) | \mathcal{D} | \Psi_0 \rangle \right|^2 \delta(\omega - E + E_0), \tag{5}$$

where $c \simeq 137$ is the speed of light in atomic units.

The dipole electromagnetic operator $\mathcal{D}$ can be written in the length or velocity gauge:

$$\mathcal{D}^r = \omega(\boldsymbol{r}_1 + \boldsymbol{r}_2)\cdot\hat{\boldsymbol{e}}, \quad \mathcal{D}^{\boldsymbol{\nabla}} = (\boldsymbol{\nabla}_1 + \boldsymbol{\nabla}_2)\cdot\hat{\boldsymbol{e}}.$$

Here $\hat{\boldsymbol{e}}$ is the polarization vector of the photon. The dipole matrix element entering Eq. (5) is calculated in the CCC formalism as

$$\langle \Psi_j^{(-)}(\boldsymbol{k}_b) | \mathcal{D} | \Psi_0 \rangle = \langle \boldsymbol{k}_b^{(-)} j | \mathcal{D} | \Psi_0 \rangle + \sum_i \Xint- d^3k \frac{\langle \boldsymbol{k}_b^{(-)} j | T | i\boldsymbol{k}^{(+)} \rangle \langle \boldsymbol{k}^{(+)} i | \mathcal{D} | \Psi_0 \rangle}{E - \varepsilon_k - \epsilon_i + i0}. \tag{6}$$

Here the channel wave function $\langle \boldsymbol{k}_b^{(-)} j |$ is the product of a one-electron target orbital $\varphi_j$ with energy $\epsilon_j$ and a (distorted) Coulomb outgoing wave $\chi^{(-)}(\boldsymbol{k}_b)$ with energy $\varepsilon_k$. As in the case of helium, the target orbital is generated with the asymptotic charge being 2, and the asymptotic charge experienced by the Coulomb wave is 1.

The square-integrable basis set of the target states $\phi_n^N$ is obtained by diagonalizing the target Hamiltonian $H_T$ in a large Laguerre (Sturmian) basis of size $N$,

$$\langle \varphi_m^N | H_T | \varphi_n^N \rangle = \epsilon_n^N \delta_{mn}. \tag{7}$$

The target two-electron Hamiltonian is defined as

$$H_T = \sum_{i=1,2} \left( -\frac{1}{2}\nabla_i^2 + V_i^{\rm FC} \right) + \frac{1}{|\boldsymbol{r}_1 - \boldsymbol{r}_2|}. \tag{8}$$

The nonlocal frozen core potential $V^{\rm FC}$ is the sum of nucleus, static Coulomb, and exchange terms:

$$V^{\rm FC}\varphi_\alpha(\boldsymbol{r}) = \left( -\frac{Z}{r} + 2\sum_{\varphi_j \in C} \int d^3r' \frac{|\varphi_j(\boldsymbol{r}')|^2}{|\boldsymbol{r} - \boldsymbol{r}'|} \right) \varphi_\alpha(\boldsymbol{r}) - \sum_{\varphi_j \in C} \int d^3r' \frac{\varphi_j^*(\boldsymbol{r}')\varphi_\alpha(\boldsymbol{r}')}{|\boldsymbol{r} - \boldsymbol{r}'|} \varphi_j(\boldsymbol{r}). \tag{9}$$

Here the core orbitals $\varphi_j \in C$ are obtained by performing a self-consistent-field Hartree-Fock calculation [24] for the ground state of the doubly charged ion.

The contribution from the final channels $\langle \boldsymbol{k}_b^{(-)} j |$ is separated into single and double ionization according to the energy $\epsilon_j$ which is positive for the doubly ionized channels and negative for the singly ionized channels. We also ensure that for the negative-energy-state cross sections, contributions to the ionization plus excitation cross sections are multiplied by the projection of the state onto the true target discrete subspace as is done for electron-impact ionization [25].

The fully differential DPI TDCS is calculated from the dipole matrix element $\langle \Psi(\boldsymbol{k}_1, \boldsymbol{k}_2) | \mathcal{D} | \Psi_0 \rangle$ between the ground state and the two-electron continuum. This matrix element can be obtained from the set of matrix elements (6) by projecting the distorted wave $\langle \boldsymbol{k}_2^{(-)} |$ onto the target pseudostate of matching energy $\epsilon_j = k_2^2/2$ in all partial wave channels. It is convenient to parametrize the TDCS by a pair of symmetrized amplitudes $f^{\pm}(\theta_{12}, E_1, E_2)$ which depend on the relative interelectron angle and energy [26,27]:

$$\frac{d^3\sigma}{d\Omega_1 d\Omega_1 dE_2} = \frac{4\pi^2 k_1 k_2}{\omega c}\left|\langle\Psi(\boldsymbol{k}_1,\boldsymbol{k}_2)|\mathcal{D}|\Psi_0\rangle\right|^2$$

$$= \left|[f^+(\hat{\boldsymbol{k}}_1+\hat{\boldsymbol{k}}_2)+f^-(\hat{\boldsymbol{k}}_1-\hat{\boldsymbol{k}}_2)]\cdot\hat{\boldsymbol{e}}\right|^2. \quad (10)$$

Here $\hat{\boldsymbol{k}}_i=\boldsymbol{k}_i/k_i$, $i=1,2$, are the unit vectors directed along the photoelectron momenta $\boldsymbol{k}_i$. Under the equal-energy-sharing condition, the antisymmetric amplitude vanishes $f^-(E_1=E_2)=0$ and all the information about the DPI process is contained in one symmetric amplitude $f^+$. Following predictions of the Wannier-type theories [28,29], this amplitude can be represented by a Gaussian ansatz

$$|f^+|^2 \propto \exp\left(-4\ln 2\frac{(\pi-\theta_{12})^2}{\Delta\theta_{12}^2}\right), \quad (11)$$

where the width parameter $\Delta\theta_{12}$ indicates the strength of angular correlation in the two-electron continuum. Although the analytical theories [28,29] validate Eq. (11) only near the double-ionization threshold, numerical models [30] and direct measurements [31,32] support its validity in a far wider photon energy range.

The number of the states $N$ in the Laguerre basis (7) was increased until satisfactory convergence was achieved. In practice, our calculations were performed with at least $45-l$ target states where $l=0,\ldots,l_{\max}$ is the angular momentum of the target orbital and $l_{\max}=8$. Higher values of the $l_{\max}$ are required for alkaline-earth-metal atoms as compared with He because of a larger radial extent of the target orbitals bound to the corresponding singly charged ion.

## III. RESULTS

### A. Integrated cross sections

#### 1. Beryllium

In their recent paper, Wehlitz *et al.* [5] reported cross-section data for both single and double photoionization of Be from threshold to 40 eV photon energy range with improved statistics and energy resolution. This provides our CCC model with a stringent test not available at the time of our previous publication [4]. Therefore we feel it necessary to reexamine our earlier Be data in the present work.

In Fig. 1 we present the single-photoionization cross section calculated in two gauges of the electromagnetic interaction, the length and velocity. If the ground- and final-state wave functions were exact, these two calculations would produce identical results. In practice, there is some deviation between the two gauges, especially at low photon energies. We believe this deviation is due to the frozen core approximation employed in the present work. Indeed, by taking into account the intershell correlation between the $1s^2$ and $2s^2$ shells within the random phase approximation with exchange (RPAE) [23], we were able to produce identical results in both gauges even with a noncorrelated ground state. Unfortunately, RPAE calculations can only be performed for single photoionization and cannot be used in the present DPI study.

Experimental data of Wehlitz *et al.* [5] are consistent with the present CCC calculation with a somewhat better agreement with the length gauge near the double-ionization threshold. All calculations tend to converge further away from the threshold where they are in good agreement with the earlier measurement of Wehlitz and Whitfield [3].

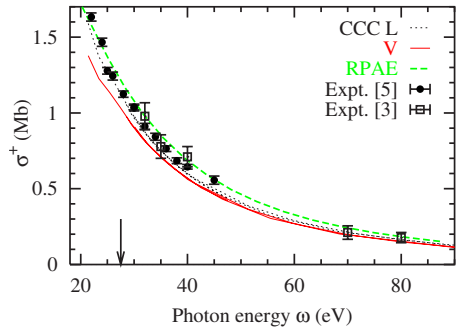


FIG. 1. (Color online) Single-photoionization cross section of Be as a function of the photon energy. The CCC calculations in the length and velocity gauges are shown by the black dotted and red solid lines, respectively. The RPAE calculation in two gauges (indistinguishable) is shown by the green dashed line. Experimental data of Wehlitz *et al.* [5] and Wehlitz and Whitfield [3] are displayed by filled circles and open squares, respectively. The arrow indicates the double-ionization threshold.

In Fig. 2 we present the double-to-single photoionization cross-section ratio in Be. We plot the present CCC calculation in the velocity gauge along with an earlier calculation reported in Ref. [4]. CCC calculations in the length gauge are not reliable for alkaline-earth-metal atoms due to the poor quality of the MCHF ground state and are not shown in the figure. We compare the CCC calculations with the experimental data of Wehlitz *et al.* [5] and Wehlitz and Whitfield [3]. Wehlitz *et al.* [5] noticed that the experimental double-to-single ratio in Be can be scaled to the analogous ratio in He [33] when plotted versus the excess energy $\Delta E$ in units of the ionization potential of the corresponding singly charged ion ($Be^+$ or $He^+$). One possible explanation of this scaling was that the DPI near threshold should proceed mainly via the electron impact ionization of the singly

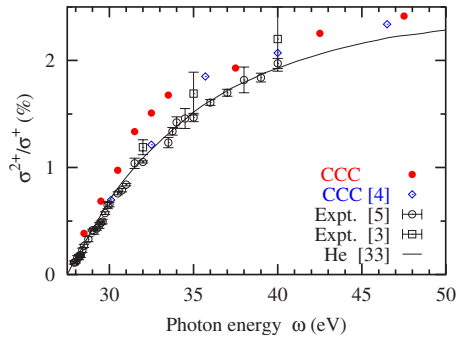


FIG. 2. (Color online) Double-to-single photoionization cross-section ratio in Be as a function of the photon energy. Present CCC calculation in the velocity gauge is plotted by red filled circles. Previous CCC results [4] are shown by blue open diamonds. Experimental data of Wehlitz *et al.* [5] and Wehlitz and Whitfield [3] are displayed by open circles and squares, respectively. The black solid line is the experimental double-to-single ratio in He [33] multiplied by 0.64 and plotted versus the excess energy in units of the ionization potential of $He^+$.

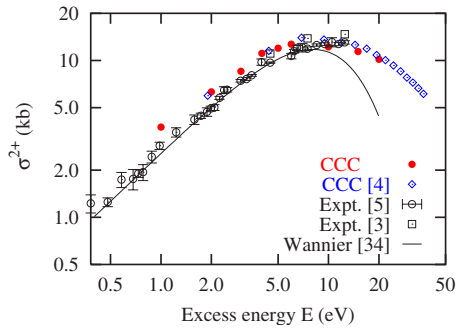


FIG. 3. (Color online) Double-photoionization cross section of Be as a function of excess energy above the double-ionization threshold. The key is the same as in Fig. 2 except for the solid line, which shows the fit of experimental data with the fourth-order Wannier theory [34].

charged ion. The cross section of the former process is a universal function of the reduced excess energy for all hydrogen like targets.

We adopt this scaling and compare in Fig. 2 the CCC double-to-single ratios of Be and He in the reduced coordinates. We see that the scaled He measurement [33] agrees very well with the Be experiment whereas the Be calculation is somewhat higher. To a certain extent, this disagreement might be due to the reduced single-photoionization cross section in the velocity gauge clearly visible in Fig. 1.

To separate double and single photoionization more clearly, we plot in Fig. 3 the absolute double-photoionization cross section of Be from both the CCC calculations and the experiments of Wehlitz and co-workers. As in Ref. [5], the experimental data are fitted with the fourth-order Wannier theory of Feagin [34]. The CCC calculation in the velocity gauge is generally consistent with the experimental data. However, the calculated cross sections are systematically larger than the experiment at the excess energies below 10 eV.

### 2. Magnesium and calcium

Unlike Be, heavier alkaline-earth-metal atoms, Mg and Ca have a subvalent $(n-1)p$ shell which can affect photoionization of the valence $ns$ shell. This effect can be particularly strong in Ca due to proximity of the giant $3p \rightarrow 3d$ resonance at 31.4 eV to the double-ionization threshold. We cannot account for intershell electron correlation in the presently employed frozen core model. However, we can examine this effect in the single photoionization channel where we can perform a separate RPAE calculation.

The single-photoionization cross sections of Mg and Ca near the corresponding double-ionization threshold are presented in Fig. 4. Three calculations are shown in the figure. In the one-channel RPAE calculation, only ionization of the valence shell $ns \rightarrow \epsilon p$ is taken into account. In a more sophisticated RPAE calculation, the intershell electron correlation is taken into account by mixing three photoionization channels: $ns \rightarrow \epsilon p$ and $(n-1)p \rightarrow \epsilon s$, $\epsilon d$. In Mg, the difference between the two RPAE cross sections does not exceed 15%. The CCC calculation is close to the one-channel RPAE. The

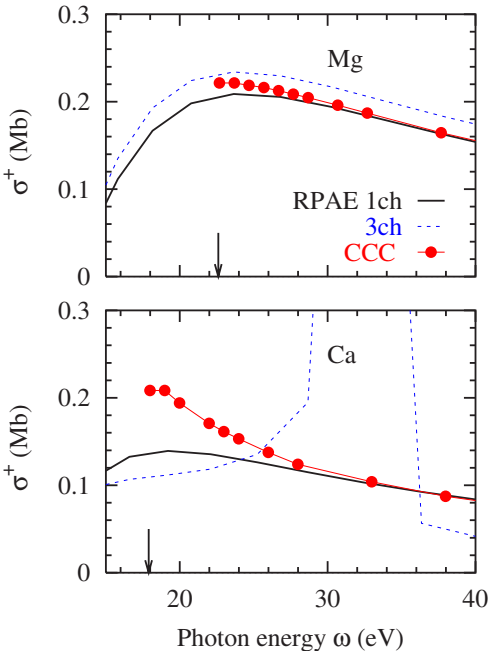


FIG. 4. (Color online) Single-photoionization cross sections of Mg (top) and Ca (bottom) as a function of the photon energy. RPAE calculations with one and three channels are shown by the black solid and blue dashed lines, respectively. The three-channel RPAE calculation for Ca is scaled down by a factor of 0.2. The CCC calculation is shown with the red circles. The corresponding double ionization thresholds are indicated by arrows.

situation is completely different in Ca where the $4s$ photoionization cross section is dominated entirely by the giant $3p \rightarrow 3d$ resonance. Unfortunately, the CCC frozen core model cannot account for this effect. Although we did not probe explicitly the DPI channel, it is fair to assume that the intershell correlation would play a similar role there. This means that the present Ca results should be treated as model-specific calculations and a certain care should be exercised when comparing these data with experiment. In the meantime, the DPI calculations on Mg can be considered as accurate as those on Be.

The double-to-single photoionization cross-section ratio for Mg and Ca is presented in Fig. 5 in comparison with unpublished preliminary results of Nagata [35]. There is a strong disagreement between the theory and experiment for both targets. The calculated ratio in Mg seems to be too low whereas the same ratio in Ca is too high as compared with the experiment. On the basis of single-photoionization calculations, we can expect the CCC ratio in Mg to be accurate within 15% which is far exceeded by a nearly fourfold difference from the experiment. Wehlitz [36] communicated to us his unpublished and still preliminary set of ratios in Mg which flatten at about the same photon energy as predicted by the CCC calculation and reach the peak value close to 1%. This later set of experimental data seems to be in a much closer agreement with our calculation.

In Fig. 6 we compare the double-to-single photoionization cross-section ratios of all presently studied alkaline-earth-metal atoms with that ratio in He. The same reduced excess energy scale is used measured in units of the ionization po-

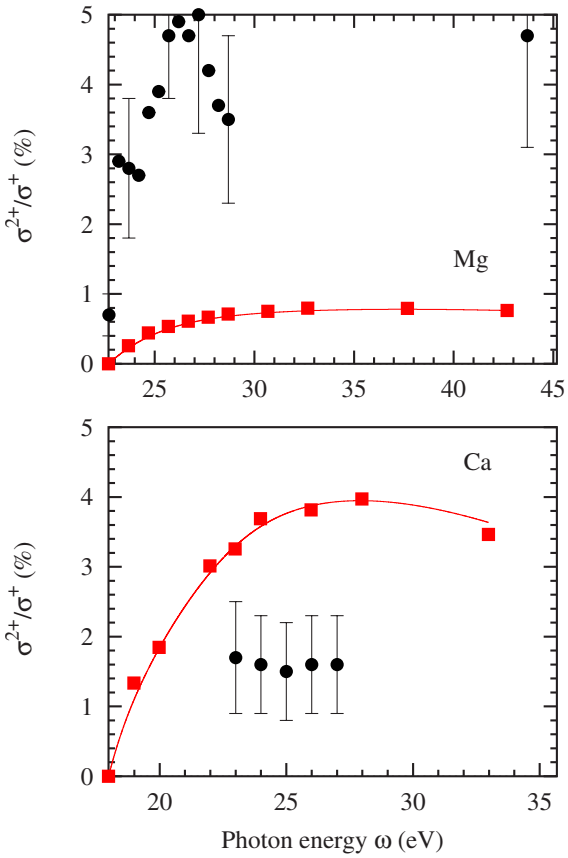


FIG. 5. (Color online) Double-to-single photoionization cross-section ratios in Mg (top) and Ca (bottom) as functions of the photon energy. Present calculation (red filled squares) is shown in comparison with experimental data of Nagata [35]. The red solid line is a smooth interpolated curve to guide the eye through the calculated data.

tential of the corresponding singly charged ion: 54.4 eV for $He^+$, 18.2 eV for $Be^+$, 15.0 eV for $Mg^+$, and 11.8 for $Ca^+$ [2]. The corresponding photon energy scale in eV is indicated on the top horizontal scale of each panel. On the helium plot (top left panel) we show the experimental double-to-single ratio [33]. To test the scaling of this ratio to the electron-impact ionization cross section of the $He^+$ ion, we draw in the same figure the theoretical $(e,2e)$ cross section [37] which was found in perfect agreement with the experimental data [38,39]. This cross section is plotted versus the reduced excess energy and scaled to the photoionization cross-section ratio near the double-ionization threshold.

As was already observed by Samson [43] and later reiterated by Wehlitz *et al.* [5], both curves have indeed a similar shape from the threshold up to $\Delta E \simeq 0.5$. We note, however, that the electron impact ionization of $He^+$ is dominated by nondipole partial waves which are forbidden in the photoionization process. To illustrate this fact, we present in the figure a restricted $(e,2e)$ calculation in which all nondipole contributions are suppressed and only the total angular momentum $J=1$ of the scattering system ion plus electron is allowed. To place this calculation on the common scale we have to apply a scaling factor which is 7.7 times larger than the same factor for the unrestricted $(e,2e)$ calculation in which all $J$ are allowed. This means that the dipole channel contributes only about 13% of the total $(e,2e)$ cross section. As it was argued in Ref. [44], it is this, dipole-only, $(e,2e)$ cross section that should be scaled versus the double-photoionization cross-section ratio. This scaling applies in a somewhat narrower energy range from the threshold to $\Delta E \simeq 0.3$. Outside this range, the contribution of the other, shake-off mechanism upsets the scaling between the $(\gamma,2e)$ and $(e,2e)$ reactions.

Similar data presentation is used in other panels where we show the double-to-single photoionization cross-section ratio for Be (top right), Mg (bottom left), and Ca (bottom right). The present calculation is compared with a scaled ratio for He [33] which is multiplied by 0.80, 0.37, and 1.5 in the Be, Mg, and Ca plots, respectively. The electron impact ionization of the corresponding singly charged ion is taken from experiment (Ref. [40] for Be, Ref. [41] for Mg, and Ref. [42] for Ca). Dipole-only $(e,2e)$ cross-section is extracted from the same CCC calculation as the double-to-single photoionization cross-section ratio.

We observe that, in extended excess energy range up to $\Delta E \simeq 1.0$, the scaled $(e,2e)$ cross section on each target follows closely the double-to-single photoionization cross-section ratio of He. We can offer no explanation to this phenomenon and find it coincidental. The cross-section ratios in alkaline-earth-metal atoms follow the analogous ratio in He at excess energy range up to $\Delta E \simeq 0.3$. In Be and Ca, this is the same range where the dipole-only $(e,2e)$ cross section scales to the photoionization cross-section ratio. In Mg, the latter scaling is extended across the whole excess energy range shown on the plot. Such a scaling indicates the range of photon energies where the electron impact ionization of the singly charged ion is the dominant mechanism of DPI. The alternative shake-off mechanism contributes insignificantly in this range.

Characteristic values of the photoionization cross-section ratios in Be and Mg at the excess photon energy range $\Delta E \simeq 1$ are smaller then in He. This goes in line with reduction of the asymptotic $R_\infty$ ratio in this sequence of targets. However, Ca breaks away from this tendency and exhibits a double-to-single ratio greater than that in He. This could possibly be explained by an electron-impact ionization cross section on $Ca^+$ which is significantly larger than that on $He^+$.

### B. DPI amplitudes

Modulus of the symmetric amplitude $f^+$ of DPI on Be is shown in Fig. 7 for selected excess energies of 20, 4, and 1 eV shared equally between the photoelectrons. The fit with a Gaussian ansatz Eq. (11) is also shown in the figure. The quality of the fit is very good on the middle panel with deviation from the Gaussian hardly visible on the scale of the figure. The fit somewhat deteriorates on the top and bottom panels, but for different reasons. The top panel represents the amplitude taken quite far away from the DPI threshold at the reduced excess energy of $E/V^+_{\rm ion}=1.1$. We note that the same excess energy of 20 eV would correspond to $E/V^+_{\rm ion}=0.37$ in He. The amplitude shown on the bottom panel is taken very close to the threshold. Here, the noticeable wings of the amplitude near zero mutual angle are most likely a numerical

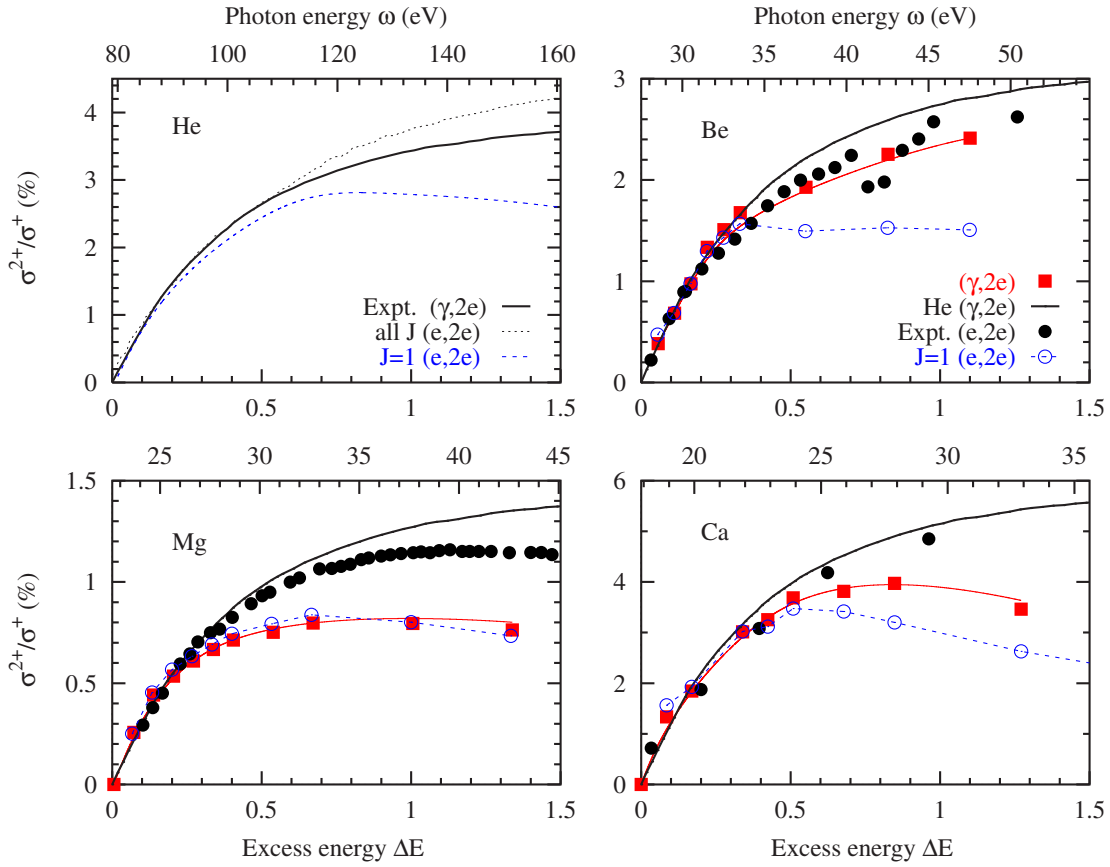


FIG. 6. (Color online) Double-to-single photoionization cross-section ratios in He, Be, Mg, and Ca as functions of the reduced excess energy $\Delta E = E/V_{\text{ion}}^{+}$ measured in units of the ionization potential of the corresponding singly charged ion. The photon energy in eV is indicated on the top horizontal scale of each plot. The data points (red filled squares) are interpolated by a smooth curve (red solid line) to guide the eye through the data. The experimental double-to-single ratio in He [33] (multiplied by 0.8, 0.4, and 1.5 to scale the Be, Mg, and Ca ratios, respectively) is shown on each plot as a thick solid line. Also shown are the electron-impact ionization cross sections of the corresponding ions (CCC calculation for He [37], black dotted line; experimental data for Be [40], Mg [41], and Ca [42], filled circles) and the theoretical dipole-only electron-impact ionization cross sections for each target ion (blue dashed lines).

artifact. The symmetric amplitude should be zero at this angle as emission of the two equal-energy electrons in the same direction is prohibited. However, in the CCC formalism, the two electrons are explicitly distinguishable. It is the full numerical convergence that assures a complete cancellation of the DPI amplitude at zero mutual angle. The excess energy of $\simeq 1$ eV represents the lower limit of the present calculation where this convergence can be confidently reached.

Although not shown in the figure, the same Gaussian shape of the symmetric amplitude $f^{+}$ can be observed in other alkaline-earth-metal atoms (Mg and Ca). This is in contrast to predictions of Kazansky and Ostrovsky[14] who reported a double-hump structure of $|f^{+}|^2$ in all alkaline-earth-metal atoms in the range of excess energies from 0.5 to 5 eV.

The Gaussian width parameter as a function of excess energy for Be and other alkaline-earth-metal atoms is shown in Fig. 8 in comparison with the width parameter of He. As in Fig. 6, we use the reduced excess energy scale $\Delta E = E/V_{\text{ion}}^{+}$ measured in units of the ionization potential of the corresponding singly charged ion.

First, we observe a significant reduction of the Gaussian width parameter in alkaline-earth-metal atoms as compared with He. This reduction was already reported in previous calculations on Be [6,30]. However, the origin of this reduction was attributed to different factors. Citrini *et al.* [6] explained it in terms of a greater ground-state correlation in Be as compared to He. Conversely, it was argued in Ref. [10] that this effect had little to do with electron properties of the neutral target. Rather, it could be explained by the narrowing width of the momentum profile of the bound electron attached to the corresponding singly charged ion.

In Fig. 9 we plot the momentum profiles (squared momentum space wave functions) $|R_{ns}(q)|^2$ of the valence $ns$ states in $He^{+}$ ($n=1$), $Be^{+}$ ($n=2$), $Mg^{+}$ ($n=3$), and $Ca^{+}$ ($n=4$). All the momentum profiles are normalized to $|R_{1s}|^2$ of $He^{+}$ at its maximum. We see that, indeed, the width of the momentum profile is receding monotonically from He to Ca, hand in hand with the Gaussian width parameters in Fig. 8. To quantify this reduction, we took the Gaussian width in all the targets at a fixed, somewhat arbitrarily, reduced excess energy of $\Delta E = 0.3$ and plotted it versus the momentum width at half maximum $\Delta q$ extracted from the momentum profiles of Fig. 9. The resulting dependence is shown in Fig. 10. The calculated data points in Fig. 8 are somewhat scattered. So the width parameters presented in Fig. 10 are supplied with

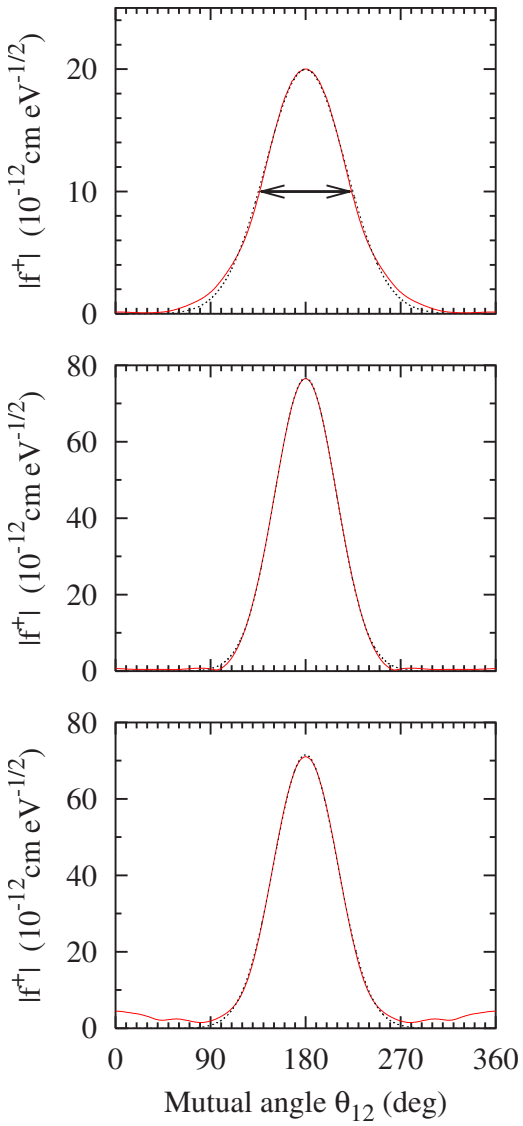


FIG. 7. (Color online) Modulus of the symmetric amplitude $f^+$ of DPI on Be at equal energy sharings of $E_1=E_2=10$, 2, and 0.5 eV (from top to bottom) is shown by the red solid line. Each amplitude is fitted with a Gaussian displayed by a black dotted line. The arrow indicates the Gaussian width parameter $\Delta\theta_{12}$ in Eq. (11).

"error bars" extracted from the interpolation procedure. Within these error bars, the calculated points in Fig. 10 can be approximated by the $\Delta\theta_{12} \propto \Delta q^{3/4}$ dependence.

In addition to the systematic reduction of the Gaussian width, we observe in Fig. 8 a nonmonotonic dependence of the width versus the excess energy in the alkaline-earth-metal atoms in contrast to that in He. The width, as a function of the excess energy, displays a shallow minimum at $E \approx 0.3V_{\text{ion}}^+$. This behavior is unexpected. The Wannier threshold law for the angular correlation width is $\Delta\theta_{12} \propto E^{1/4}$ [28,29]. The He data seem to approach the Wannier regime at quite small excess energies of the order of $E \simeq 0.01V_{\text{ion}}^+$. Other alkaline-earth-metal atoms have much smaller ionization potentials of the singly charged ions and the regime of very small $\Delta E \sim 0.01$ cannot be reached in the present calculation.

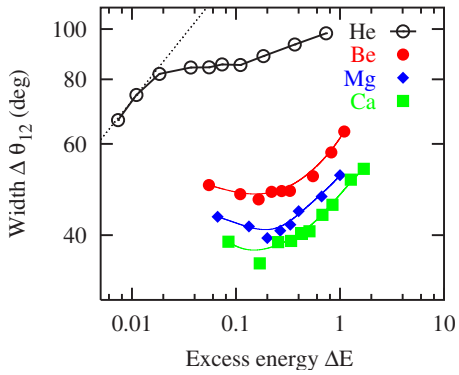


FIG. 8. (Color online) Gaussian width parameter $\Delta\theta_{12}$ as a function of the reduced excess energy $\Delta E = E/V_{\text{ion}}^+$ for various alkaline-earth-metal atoms (Be, red circles; Mg, blue diamonds; Ca, green squares) and helium (black open circles). The correspondingly colored solid lines are smooth interpolated curves to guide the eye through the calculated data. The dotted line indicates the onset of the Wannier threshold law proportional to $E^{1/4}$ for He.

### C. Triply differential cross section

Knowledge of the ionization amplitude allows one to generate the fully resolved TDCS for arbitrary polarization of light, geometry of two-electron escape, and energy sharing between the photoelectrons. In Fig. 10 (middle panel), we present the TDCS of Ca at the excess energy of 25 eV shared equally between the photoelectrons. Comparison is made with experiment of Beyer *et al.* [12] in which the fixed-angle electrons were ejected parallel to the electric vector of 100% linearly polarized light. In the same figure (bottom panel) we present analogous TDCS results for He calculated at the same geometry. The excess energy $E=20$ eV is chosen somewhat lower to make a comparison with the experimental data of Bräuning *et al.* [45]. To facilitate analysis of the TDCS results, on the top panel of the figure we plot the symmetric DPI amplitudes of Ca and He at the correspond-

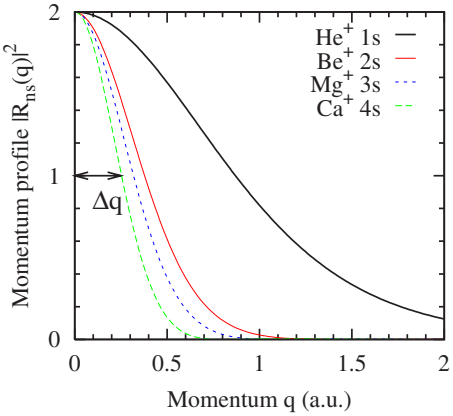


FIG. 9. (Color online) Momentum profiles (squared momentum space wave functions) $|R_{ns}(q)|^2$ of the valence $ns$ state in $He^+$ ($n=1$, black thick solid line), $Be^+$ ($n=2$, red solid line), $Mg^+$ ($n=3$, blue short-dashed line), and $Ca^+$ ($n=4$, green long-dashed line). The momentum profiles are normalized to $|R_{1s}|^2$ of $He^+$ at its maximum. The arrow indicates the extraction of the momentum width at half maximum $\Delta q$.

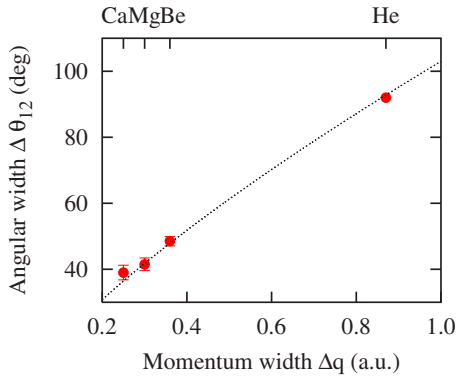


FIG. 10. (Color online) Gaussian angular width parameter $\Delta\theta_{12}$ taken at the reduced excess energy $\Delta E=E/V_{\rm ion}^{+}=0.3$ versus the momentum width at half maximum $\Delta q$ in He and various alkaline-earth-metal atoms. The dotted line is the fit with the power law $\Delta\theta_{12}\propto\Delta q^{3/4}$.

ing excess energies. As the fixed electron is detected at zero angle $\theta_1=0°$, the variable angle $\theta_2$ is equal to the mutual electron angle $\theta_{12}=\theta_2-\theta_1$ and all three plots can be aligned to the same $x$ scale.

The symmetrized amplitude in He has a nearly perfect Gaussian shape with a width parameter of $\Delta\theta_{12}\simeq 95°$. The corresponding TDCS has a single maximum at $\theta_{12}\simeq 100°$. This maximum is reached as a "compromise" between the amplitude (dynamical factor) which has a maximum at $\theta_{12}=180°$ and the kinematical factor $\cos\theta_1+\cos\theta_2$ which has a node at this angle.

The central part of the symmetrized amplitude in Ca has a Gaussian shape as well with a much narrower width parameter of $\Delta\theta_{12}\simeq 56°$. The sharp peak of the amplitude at $\theta_{12}=180°$ gives rise to a maximum of the TDCS at about $\theta_{12}\simeq 135°$. This is visualized by the black solid line which represents the TDCS generated from the Gaussian fit to the symmetric amplitude shown on the top panel of Fig. 10. In deviation from a Gaussian, this amplitude has a little hump at $\theta_{12}\simeq 100°$. This non-Gaussian feature is due to a much larger reduced excess energy of $E/V_{\rm ion}^{+}=2.1$ as compared to only 0.36 in He which means that the Ca data are taken much further away from the threshold where the Gaussian parametrization does not hold so well. The additional feature of the amplitude gives rise to a bold maximum of TDCS at $\theta_{12}\simeq 105°$. Experimental data show a single maximum which is roughly between the two maxima on the theoretical curve. We should note that the TDCSs presented in Fig. 11 correspond to the photon energy of 36.8 eV, which is very close to the giant $3p\rightarrow 3d$ resonance at 31.4 eV, which can modify strongly the present frozen-core calculation.

## IV. CONCLUSION

In the present paper we report on the convergent close-coupling calculations of double photoionization of alkaline-earth-metal atoms Be, Ca, and Mg. Our model comprises the MCHF expansion of the valence shell of the target atom and the CCC expansion of the two-electron continuum in the Hartree-Fock field of the ionized target. In both the ground

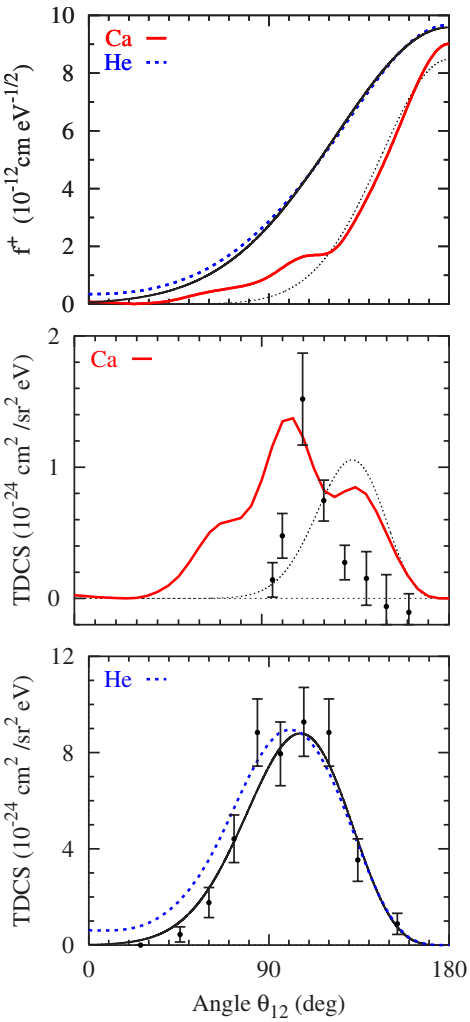


FIG. 11. (Color online) Top panel: symmetric DPI amplitudes $f^{+}(\theta_{12},E_1,E_2)$ at $E_1=E_2=12.5$ eV in Ca (red solid line) and at $E_1=E_2=10$ eV in He (blue dotted line) plotted versus the mutual electron angle $\theta_{12}$. Both amplitudes are fitted with the Gaussian ansatz Eq. (11) shown by the black solid (He) line and dotted (Ca) lines. Middle panel: DPI TDCS of Ca at $E_1=E_2=12.5$ eV at fixed electron angle $\theta_1=0$ plotted versus $\theta_{12}$. Experimental data from Ref. [12] on relative scale are normalized to the calculation. Bottom panel: same for He at $E_1=E_2=10$ eV. Absolute experimental data are from Ref. [45]. The black solid line on the middle panel and black dotted line on the bottom panel indicate the TDCS generated from the Gaussian fit to the corresponding symmetric amplitudes shown on the top panel.

state and the final ionized state, the core (and subvalent) electrons are kept frozen.

As a test bench, we use the recent accurate measurement of the single- and double-photoionization cross sections in Be [5]. Our data are in a reasonable agreement with experiment. For the single-photoionization cross section, the theory is about 10% below the experimental data near the DPI threshold, but comes into better agreement further away from the threshold. By relaxing the core and calculating the cross section in the RPAE approximation, we can bring the theoretical cross section into perfect agreement with the experiment. This kind of calculation, however, is only available for

single photoionization. For double photoionization, our CCC calculation in the velocity gauge is about 20% higher than the experiment near the threshold. Agreement is somewhat better at excess energies above 10 eV.

Having tested our model, we proceed with calculations for other atoms, Mg and Ca. We use the notion of the reduced excess energy measured in units of the ionization potential of the singly ionized target. This allows us to bring alkaline-earth-metal atoms and He onto a common scale. On this scale, the double-to-single photoionization cross-section ratio in all the targets follows a universal shape function. This scaling was already noticed in earlier publications [5,43]. It was attributed to the fact that the DPI process near threshold in all two-electron targets is dominated by the electron-impact ionization of the corresponding singly charged ion. The cross section of the latter process can be scaled to a universal shape function. Although we generally subscribe to this interpretation, we find two important differences. First, scaling of the double-to-single photoionization cross-section ratios is observed in a much reduced excess energy range from the threshold to $\Delta E \simeq 0.3$. Second, it is the dipole-only $(e,2e)$ cross section that should be taken for the electron-impact ionization process.

The magnitude of the double-to-single photoionization cross-section ratio in He and alkaline-earth-metal atoms is a result of interplay of two DPI mechanisms: shake-off and $(e,2e)$ on singly charged ions. The former process can be characterized by the asymptotic ratio $R_\infty$ taken in the limit of infinite photon energy. This ratio is decreasing from He to Ca due to increasing probability of the second target electron to remain bound because of a closer overlap of the neutral and ionized target orbitals. This, in turn, is caused by a shielding effect of the other core and subvalent electrons. On the contrary, the electron-impact ionization cross section of the singly charged ion is growing from $He^+$ to $Ca^+$ due to increasing size of the valence orbital in the coordinate space. These two competing tendencies result in reduction of the double-to-single photoionization cross-section ratio from He to Mg but its bouncing back in Ca.

To further our understanding of DPI process, we extract the symmetrized DPI amplitudes in alkaline-earth-metal atoms and compare them with He. We concentrate on a special case of the equal energy sharing when only one fully symmetric amplitude is needed to generate the TDCS. In the range of excess energy not exceeding the corresponding ionization potential of the singly charged ion $\Delta E = E/V_{\rm ion}^+ \leqslant 1$, the amplitudes can be fitted with a Gaussian ansatz. The Gaussian width parameter in all the alkaline-earth-metal atoms studied here is much smaller than in He at the corresponding reduced excess energy. We explain this decrease by narrowing the width of the momentum profile of the valence *ns* orbital in the corresponding singly charged ion. This corresponds to a more diffuse orbital in the coordinate space shielded by other core and subvalent electrons from the nucleus. The alternative explanation put forward by Citrini *et al.* [6] cannot be ruled out because the ground-state correlation is indeed stronger in alkaline-earth-metal atoms than in He. However, because of the close relation of the DPI and electron-impact ionization of the singly charged ion which manifests itself in scaling of the integrated cross sections, we would argue that the former cause is more likely than the latter.

Unlike in He, the Gaussian width parameter in the alkaline-earth-metal atoms is not a monotonic function of excess energy and has a shallow minimum at $E \approx 0.3 V_{\rm ion}^+$. This behavior is at odds with the Wannier threshold law which predicts a monotonic decrease $\Delta\theta_{12} \propto E^{1/4}$. On the one hand, the observed minimum can be outside the range of validity of the Wannier law whose onset takes place in He at $E \simeq 0.01 V_{\rm ion}^+$. On the other hand, Lukic *et al.* [8] reported a noticeable deviation from the Wannier regime in Be in the form of an oscillating DPI cross section which they attributed to the Coulomb dipole field of the singly ionized target. Unfortunately, in the present study, we cannot reproduce these results because our calculation becomes poorly converged and lacks sufficient accuracy at very small excess energies close to the threshold.

To summarize our finding, we note that, in the excess energy range studied here, DPI of alkaline-earth-metal atoms resembles qualitatively that of helium. A quantitative difference is caused by the structure of the *ns* valence orbital which has a twofold effect. A more diffuse structure in the coordinate space causes a closer overlap between the target orbitals bound to the neutral atom and the singly charged ion thus increasing the chance of the target electron to remain bound and decreasing the probability of DPI. Second, narrowing of the momentum profile of the *ns* orbital bound to the singly charged ion reduces the angular correlation width in the two-electron continuum. Increasing strength of the ground-state correlation from He to Be and further still to Mg and Ca may also play a role.

In addition to these qualitative differences, we observed a quantitative effect present in DPI of alkaline-earth-metal atoms and absent in He. The correlation width parameter is not a monotonic function of excess energy and has a shallow minimum. This observation contradicts the Wannier threshold law. However, the onset of the threshold law may be at a lower excess energy range, not accessible in the present study.

We finally note that the present Ca results are obtained within the frozen core model which cannot account for the strong intershell correlation between the valence $4s^2$ and subvalent $3p^6$ shells. To make theoretical predictions that can be reliably compared with experimental data, this intershell correlation should be included into the model. This development is now in progress.

## ACKNOWLEDGMENTS

We thank Ralf Wehlitz and Tetsuo Nagata for communicating their experimental results in numerical form. One of the authors (A.S.K.) wishes to thank the Japan Society for the Promotion of Science for supporting his visit to the Photon Factory. He greatly values many stimulating discussions with Professor Y. Azuma. The authors wish to thank the Australian Partnership for Advanced Computing (APAC) and ISA Technologies, Perth, Western Australia, for provision of their computing facilities. Support of the Australian Research Council in the form of Discovery Grant No. DP0451211 is acknowledged.

[1] K. G. Dyall, I. P. Grant, C. T. Johnson, F. P. Parpia, and E. P. Plummer, Comput. Phys. Commun. **55**, 425 (1989).
[2] A. A. Radzig and B. M. Smirnov, *Reference Data on Atoms, Molecules, and Ions* (Springer-Verlag, Berlin, 1985).
[3] R. Wehlitz and S. B. Whitfield, J. Phys. B **34**, L719 (2001).
[4] A. S. Kheifets and I. Bray, Phys. Rev. A **65**, 012710 (2002).
[5] R. Wehlitz, D. Lukic, and J. B. Bluett, Phys. Rev. A **71**, 012707 (2005).
[6] F. Citrini, L. Malegat, P. Selles, and A. K. Kazansky, Phys. Rev. A **67**, 042709 (2003).
[7] J. Colgan and M. S. Pindzola, Phys. Rev. A **65**, 022709 (2002).
[8] D. Lukic, J. B. Bluett, and R. Wehlitz, Phys. Rev. Lett. **93**, 023003 (2004).
[9] A. Temkin, Phys. Rev. Lett. **49**, 365 (1982).
[10] A. S. Kheifets and I. Bray, Phys. Rev. A **73**, 020708(R) (2005).
[11] T. Osawa, Y. Tohyama, R. Kobayashi, S. Obara, Y. Azuma, and T. Nagata, in XIV International Conference on Vacuum Ultraviolet Radiation Physics, Cairns, Australia, 2004 (unpublished), p. W-Po-28.
[12] H.-J. Beyer, J. B. West, K. J. Ross, and A. D. Fanis, J. Phys. B **33**, L767 (2000).
[13] S. C. Ceraulo, R. M. Stehman, and R. S. Berry, Phys. Rev. A **49**, 1730 (1994).
[14] A. K. Kazansky and V. N. Ostrovsky, J. Phys. B **30**, L835 (1997).
[15] K. J. Ross, J. B. West, and H.-J. Beyer, J. Phys. B **30**, L735 (1997).
[16] K. J. Ross, J. B. West, H.-J. Beyer, and A. D. Fanis, J. Phys. B **32**, 2927 (1999).
[17] A. D. Fanis, H.-J. Beyer, K. J. Ross, and J. B. West, J. Phys. B **34**, L99 (2001).
[18] J. B. West, K. J. Ross, H.-J. Beyer, A. D. Fanis, and H. Hamdy, J. Phys. B **34**, 4167 (2001).
[19] F. Maulbetsch, I. L. Cooper, and A. S. Dickinson, J. Phys. B **33**, L119 (2000).
[20] L. Malegat, F. Citrini, P. Selles, and P. Archirel, J. Phys. B **33**, 2409 (2000).
[21] A. Dalgarno and A. L. Stewart, Proc. Phys. Soc. London **76**, 49 (1960).
[22] T. Pattard, J. Phys. B **35**, L207 (2002).
[23] M. Y. Amusia, *Atomic Photoeffect* (Plenum Press, New York, 1990).
[24] L. V. Chernysheva, N. A. Cherepkov, and V. Radojevic, Comput. Phys. Commun. **11**, 57 (1976).
[25] I. Bray and A. T. Stelbovics, Phys. Rev. Lett. **70**, 746 (1993).
[26] A. Huetz, P. Selles, D. Waymel, and J. Mazeau, J. Phys. B **24**, 1917 (1991).
[27] L. Malegat, P. Selles, and A. Huetz, J. Phys. B **30**, 251 (1997).
[28] A. R. P. Rau, J. Phys. B **9**, L283 (1976).
[29] J. M. Feagin, J. Phys. B **17**, 2433 (1984).
[30] A. S. Kheifets and I. Bray, Phys. Rev. A **65**, 022708 (2002).
[31] P. Bolognesi, I. Bray, A. Kheifets, L. Malegat, P. Selles, A. K. Kazansky, and L. Avaldi, J. Phys. B **36**, L241 (2003).
[32] A. Knapp *et al.*, J. Phys. B **28**, 645 (2005).
[33] J. A. R. Samson, W. C. Stolte, Z. X. He, J. N. Cutler, Y. Lu, and R. J. Bartlett, Phys. Rev. A **57**, 1906 (1998).
[34] J. M. Feagin, J. Phys. B **28**, 1495 (1995).
[35] T. Nagata (private communication).
[36] R. Wehlitz (private communication).
[37] I. Bray, I. E. McCarthy, J. Wigley, and A. T. Stelbovics, J. Phys. B **26**, L831 (1993).
[38] B. Peart, D. S. Walton, and K. T. Dolder, J. Phys. B **2**, 1347 (1969).
[39] P. Defrance, F. Brouillard, W. Claeys, and G. V. Wassenhove, J. Phys. B **14**, 103 (1981).
[40] R. A. Falk and G. H. Dunn, Phys. Rev. A **27**, 754 (1983).
[41] B. Peart, J. W. G. Thomason, and K. Dolder, J. Phys. B **24**, 4453 (1991).
[42] B. Peart, J. R. A. Underwood, and K. Dolder, J. Phys. B **22**, 2789 (1989).
[43] J. A. R. Samson, Phys. Rev. Lett. **65**, 2861 (1990).
[44] A. S. Kheifets, J. Phys. B **34**, L247 (2001).
[45] H. Bräuning *et al.*, J. Phys. B **31**, 5149 (1998).